A physical model of quantum cascade lasers: Application to GaAs, GaN and SiGe devices

P. Harrison*[1], D. Indjin[1], V. D. Jovanović[1], A. Mirčetić[2], Z. Ikonić[1], R. W. Kelsall[1], J. McTavish[1], I. Savić[1], N. Vukmirović[1,2], V. Milanović[2,1]

[1] School of Electronic and Electrical Engineering, University of Leeds, Leeds LS2 9JT, United Kingdom

[2] Faculty of Electrical Engineering, University of Belgrade, Bulevar kralja Aleksandra 73, 11120 Belgrade, Serbia and Montenegro

Received zzz, revised zzz, accepted zzz
Published online zzz

PACS 73.21.Fg, 42

The philosophy behind this work has been to build a predictive 'bottom up' physical model of quantum cascade lasers (QCLs) for use as a design tool, to interpret experimental results and hence improve understanding of the physical processes occurring inside working devices and as a simulator for developing new material systems. The standard model uses the envelope function and effective mass approximations to solve two complete periods of the QCL under an applied bias. Other models, such as k.p and empirical pseudopotential, have been employed in p-type systems where the more complex band structure requires it. The resulting wave functions are then used to evaluate all relevant carrier–phonon, carrier–carrier and alloy scattering rates from each quantised state to all others within the same and the neighbouring period. This information is then used to construct a rate equation for the equilibrium carrier density in each subband and this set of coupled rate equations are solved self-consistently to obtain the carrier density in each eigenstate. The latter is a fundamental description of the device and can be used to calculate the current density and gain as a function of the applied bias and temperature, which in turn yields the threshold current and expected temperature dependence of the device characteristics. A recent extension which includes a further iteration of an energy balance equation also yields the average electron (or hole) temperature over the subbands. This paper will review the method and describe its application to mid-infrared and terahertz, GaAs, GaN, SiGe cascade laser designs.

1 Introduction The quantum cascade laser (QCL), has demonstrated an impressive extension of the infrared frequency range. Since 2002 and the first terahertz QCL laser action [1], long wavelength GaAs/AlGaAs QCLs have demonstrated significant improvement in the maximum operation temperature and an impressive extension of the frequency range. Recently THz QCLs have been reported at wavelengths as along as 141μm (2.1THz) [2] and at 160μm (1.9THz) with the assistance of an external magnetic field [3]. Also a $\lambda \sim 79\mu$m (3.8 THz) QCL working up to 137K in pulsed mode [4] and a $\lambda \sim 94\mu$m (3.2 THz) working up to 93K as well as a $\lambda \sim 103\mu$m (2.9 THz) working up to 70K in continuous-wave mode [5, 6] have been demonstrated.

In the same time, several mid-infrared GaAs/AlGaAs QCLs devices have achieved pulsed room temperature operation such as the triple quantum well QCL [7] emitting at 9.3μm, the bound to continuum QCL [8] at 11μm and the superlattice QCL [9] at 12.6μm. Furthermore, continuous wave operation up to 150K has been recently reported [10]. However, the output characteristics of these devices are

* Corresponding author: e-mail: p.harrison@leeds.ac.uk, Phone: +44 113 343 20 43, Fax: +44 113 343 72 65

still rather poor in comparison to InP based mid-infrared QCLs, which can lase in CW regime at room-temperature [11]. To improve the performance of GaAs QCLs and understand better the physical limitations of particular designs, further investigation of the influences of relevant physical and technological parameters are required [12, 13].

Recent experience in the design of novel QCLs clearly shows that systematic and compact theoretical modelling is a necessary step towards effective practical implementation, improvements of the existing structures, and the understanding of physical processes within. These includes Monte-Carlo simulation of mid-infrared [14] and terahertz [15–17] devices, nonequilibrium Green's function formalism [18, 19], as well as self-consistent rate equations model [20–22]. Most recently this work is shifting towards designing THz QCL structures based on different material system [23–25].

THz QCLs based on GaAs/AlGaAs are not capable of emitting in the energy range around the longitudinal optical (LO) phonon energies ($E_{LO} \sim 36$ meV in GaAs), leaving the gap in the spectral scale between 30 and 40 μm. This can be overcome with the use of GaN/AlGaN which has significantly larger LO phonon energy ($E_{LO} \sim 90$meV) and very fast carrier dynamics, commonly considered to be a good candidate for the near-infrared intersubband applications.

On the other hand, recent success in realisation of GaAs/AlGaAs THz QCLs has intensified research efforts to realize analogous devices in Si/SiGe strained-layer technology. The possibility of monolithic integration of silicon based electronic and optoelectronic components is a strong incentive for this research. It is presently considered that p-type Si/SiGe structures are more promising candidates for QCLs than n-type ones, because the valence band takes a larger share of the band gap discontinuity at heterostructure interfaces. Evolving from the earlier proposals of suitable structures [26], the present status of the research includes the demonstration of successful growth of long Si/SiGe cascades, and observations of electroluminescence in the THz range [27, 28]. A bias-tunable emission wavelength has also been obtained [29], although full laser operation has yet to be achieved.

2 The model Consider a QCL structure with a large number of periods (each containing of multiple quantum well) in an externally applied electric field. The energy spectrum is formally continuous, but to a very good approximation can be considered as consisting of quasi-discrete states (resonances). Based on the wavefunction localization properties, these states can be associated to different periods of the QCL, so that each period has an identical set of N states in the energy range of interest. Electron scattering occurs between states within the same period, and between states associated to different periods, the latter clearly becoming less effective for more distant periods because of reduced wavefunction overlap. Assuming an identical electron distribution in each period, one may consider some 'central' period and take its P nearest neighbours on either side, and write the scattering rate equations in the steady-state [20] :

$$\sum_{j=1,j\neq i}^{N} n_j W_{j,i} - n_i \sum_{j=1,j\neq i}^{N} W_{i,j} + \sum_{k=1}^{P} \sum_{j=1,j\neq i}^{N} \left[n_j (W_{j,i+kN} + W_{j+kN,i}) - n_i (W_{i+kN,j} + W_{i,j+kN}) \right] = 0 \tag{1}$$

where $i+kN$ is the ith state of the kth neighbouring period, $\mathrm{W}_{i,j}$ is the total scattering rate from state i into state j, n_i is the electron concentration of the ith state. The first two sums in Eq.1 are due to intra-period, and the third due to inter-period scattering. After solving for electron densities n_i, macroscopic parameters of the system like current density and gain can be calculated. The scattering time $W_{i,f}$ is a function of both n_i and n_f, the initial and final subband populations, hence, this set of equations has to be solved self–consistently using an iterative procedure. At equilibrium, the rate at which the electron distributions gain kinetic energy (relative to the particular subband minimum) through scattering, will balance with the rate at which they lose kinetic energy to the lattice. Despite the fact that electron–electron scattering is elastic as far as total energy is concerned, intersubband electron–electron transitions do convert potential energy into kinetic energy (or vice-versa). From the viewpoint of this work this would lead to an increase

(decrease) in the total kinetic energy of a subband population, because the potential energy as defined here includes the quantised component of the kinetic energy. Hence, the kinetic energy balance condition in case where only electron-LO phonon and electron-electron processes are included, can be written as [21]:

$$\Delta = \sum_{\mathrm{em.,abs.,e-e}} \sum_{f} \sum_{i} n_i W_{i,f}(E_i - E_f + \delta E) = \Delta_{\mathrm{e-LO}} + \Delta_{\mathrm{e-e}} = 0 \tag{2}$$

where $E_i - E_f$ is the subband separation, and the change in energy δE is equal to $-E_{\mathrm{LO}}$ for phonon emission (em.), $+E_{\mathrm{LO}}$ for phonon absorption (abs.) and zero for electron–electron (e-e) scattering. Hence, $\Delta_{\mathrm{e-LO}}$ is net electron-LO phonon, and $\Delta_{\mathrm{e-e}}$ is net electron–electron contribution in the balance equation. The method is easily extendible in case that other scattering mechanisms (electron-acoustical phonon, impurity and alloy scattering, etc.) should be taken into account. The next step of the procedure, is to vary the electron temperature (assumed to be the same for all subbands) until the kinetic energy balance equation Eq. (2) is satisfied self-consistently.

The current density can be calculated by subtracting the current density component due to electrons scattering into the next periods of the QCL from the component due to electrons scattering back. If we put a reference plane somewhere in the injection barrier of the central period, the current density flowing throught that cross section can be written as:

$$J = \sum_{k=1}^{P} \sum_{i=1}^{N} \sum_{j=1}^{N} k \cdot n_i \left(W_{i,j+kN} - W_{i+kN,j} \right) \tag{3}$$

The factor k in the summation, effective for non-nearest-neighbour scattering, comes from scattering from any QCL period left of the centre period into any period right of it, or vice versa (i.e. skipping the central period, but going through the reference plane). In order to reduce the number of scattering rate processes necessary to calculate the electron distribution and the corresponding current density (note that the number of total scattering rate processes is equal to $N^2(2P+1)-N$), we introduce the 'tight-binding' approximation assuming that only a few closest neighbors interact, and set $P = 2$. The choice of quantum scattering mechanisms depends on the material and doping density, as well as wavelength. For example in the novel GaAs-based THz QCLs the energy separation between most of subbands is smaller than the LO phonon energy and electron-electron scattering becomes the dominant scattering mechanism, hence necessitating a large number of possibly relevant scattering processes to be accounted for [22]. To extract the output characteristics of QCLs, one has to change the electric field F (i.e. the applied voltage) and calculate the modal gain G_M and the total current density J for each value of the field.

3 Application Electric field vs current density characteristics at lattice temperature $T_{\mathrm{latt}} = 20K$ is shown in Fig. 1a for original terahertz QCL [1]. Under the assumption $T_{\mathrm{e}} = T_{\mathrm{latt}}$ (doted line), the $F - J$ curves show current density saturation and negative differential resistance (NDR) features at very low currents, which are not consistent with experimental results [1]. We find with the calculation (solid line), which includes the energy balance, but when only electron-electron and electron LO phonon scattering are included, that current is predicted to saturate at ~ 680 A/cm^2 in reasonable agreement with that measured at ~ 820 A/cm^2. Calculated values of the average electron temperature are also shown. The calculations also show that, up to the NDR feature, T_{e} can be approximated as linear function $T_{\mathrm{e}} \approx T_{\mathrm{latt}} + \beta J$, where $\beta \sim 52$ K/(kAcm^{-2}). The most recent micro-probe photoluminscence measurement but in a different terahertz QCLs design [30], suggest $\beta \sim 69 - 77$ K/(kAcm^{-2}) in qualitative agreement with our findings.

The extended multi-electron-temperature model [31] with impurity and interface roughness scattering mechanisms included, gives calculated saturation current of ~ 910 A/cm^2 i.e. slightly higher than the measured value of ~ 820 A/cm^2. In that case, the discrepancy is possibly due to the an overestimate of interface roughness correlation length used in the simulation. Calculation shows an even stronger increase of the upper laser level temperature T_{e2}, while the lower laser level temperature T_{e1} remained almost

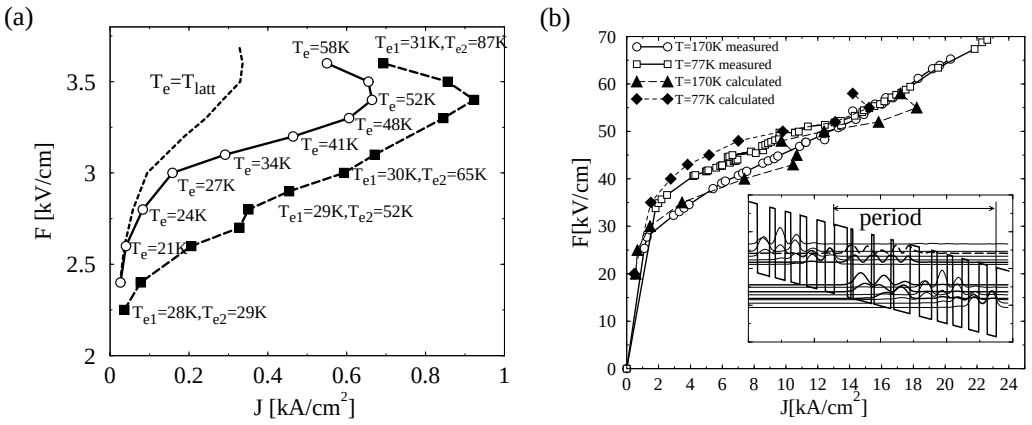

Fig. 1 (a) Calculated electric field vs. current density characteristics in the first THz QCL at lattice temperature $T_{\rm latt} = 20$. (b) The calculated and measured current-voltage characteristic of mid-infrared GaAs/$Al_{0.45}Ga_{0.55}As$ 2LO QCL at two different temperatures (T=77K and T=170K). A schematic diagram of analyzed structure is given in the inset with the layer sequence of one period (in angstrom) starting from the injection barrier: 39.2/11.2/5.6/56/8.4/50.4/8.4/50.4/28/36.4/16.8/30.8/16.8/28/19.6/30.825.2/28

constant and close to the lattice temperature, see Fig. 1a dashed line. These results are in qualitative agreement with recent measurements although in a different THz QCLs structure, based on direct LO-phonon depopulation [13], and also with recent Monte-Carlo simulation of the same device [17].

A fully optimized design of a $\lambda \sim 10\mu$m GaAs-based mid-infrared QCL (see inset of Fig. 1b) based on the mechanism of double-phonon resonance depopulation (2LO QCL) of the lower laser level, (successfully implemented in continuous wave room-temperature InP-based mid-infrared QCL [11, 32]), has been grown at the Paul Drude Institute, Berlin [33]. A very good agreement between the calculated and measured current-voltage characteristics of the device was obtained, and between the calculated and measured threshold current at 77K ($I_{th} = 2.8$A), see Fig. 1. Also, the observed emission wavelength $\lambda \approx 10.4\mu$m is in good agreement with calculated value of $\lambda \approx 10.25\mu$m. As a result of the relatively low (nonoptimised) doping density (sheet density $N_s \sim 4 \times 10^{11}$ cm^{-2}) the first sample did not reach room-temperature operation ($T_{max} = 240$K in pulsed mode).

The designs for GaN/AlGaN quantum cascade lasers emitting at 34 and 38 μm ($\Delta E \sim 36/34$ meV - GaAs forbidden Reststrahlenband) are shown in Fig. 2a, assuming the both a- and c-plane crystal growth orientation [34]. The Al content in the barriers is 25% in the a-plane (structure I) and 20 % in the c-plane (structure II) structure. To achieve full strain balance [34], these structures should be grown on (virtual) substrate with $2.5 - 3\%$ AlN, though the more common pure GaN substrate is also acceptable because of low average content of AlN in the cascade stack. The strain conditions in layers influence the potential (piezoelectrically), and this was accounted for [34].

The quasi-bound energies and associated wavefunctions are calculated with the intrinsic electric field induced by piezoelectric and spontaneous polarization for c-plane and only piezoelectric component for a-plane design included. The QCL structures were simulated and output characteristics extracted using fully self-consistent scattering rate equation model with all relevant intra- and inter-period scattering included. Both electron-LO phonon and electron-electron scattering mechanisms are taken into account. The population inversion up to 20% for a-plane and up to 25% for c-plane design is found resulting in feasible laser action [23]. These assumptions were confirmed by comparison between calculated modal gain and estimated waveguide and mirror losses, see Fig 2.

To compare the performance of the various simulation methods, example calculations have been performed for a simple p-SiGe cascade, each period of which comprises a 16 monolayer (4.41 nm) wide $Ge_{0.3}Si_{0.7}$ well and an 8 monolayer (2.15 nm) wide Si barrier, grown on a $Ge_{0.2}Si_{0.8}$ virtual substrate. It

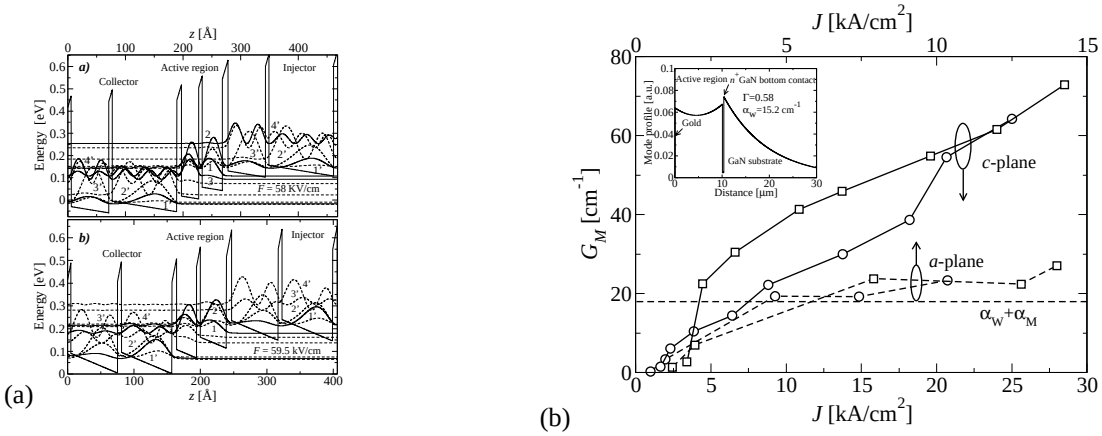

Fig. 2 (a) A schematic diagram of quasi-bound energy levels and associated wavefunctions squared for a injector-active region-collector segment ($1\frac{1}{2}$ period) of a) a-plane and b) c-plane GaN/AlGaN THz QCL. The layer sequence of one period of structures, in nanometers, from right to left from the injection barrier: **0.8**, 3, **0.6**, 3.5, **1**, 6.5, **0.6**, 11.2 for structure a) and **0.7**, 3, **0.6**, 3.9, **0.8**, 7, **0.6**, 7.6 for structure b). The normal script denotes the wells and bold the barriers. (b) Modal gain as a function of current density for a-plane (dashed line) and c-plane (solid line) designs, calculated for $T = 20$K (circles) and $T = 77$K (squares). The dashed horizontal line denotes the total waveguide and mirror losses. Inset: Single-plasmon GaN -based waveguide design and mode profile.

has just two low-lying subbands per period, the ground (HH1) and the first excited (LH1) subband, spaced by 27.5 meV, with the next (HH2) subband being much higher. In a biased cascade the alignment of the HH1 subband from the "preceding" (higher) well and the LH1 subband of the next (lower) well, both at zone centre, occurs at a field of 42 kV/cm. The structure may be interesting as a possible QCL design where the lasing transition would be the inter-well HH1→LH1(R), occurring at biases above 42 kV/cm (the energy of this transition is field-tunable), while the intra-well LH1→HH1 is the relaxation transition, emptying the lower laser state (Fig. 3a).

We have analysed this structure using the rate equations method with thermal balancing and, for comparison, with both the Monte Carlo (MC) method and simple rate equation approach [35]. Results were obtained from the simple rate equation method using two approaches: firstly, the subband carrier temperatures were simply assumed equal to the lattice temperature, and secondly, these temperatures were obtained from our Monte Carlo simulations, for each value of electric field. One of the main differences between the MC and rate equations methods is that the carrier distribution functions in each subband are generated self-consistently in the MC simulation, whereas they are always assumed to be Fermi-Dirac like in the rate equations approach. Therefore, subband carrier temperatures cannot be precisely defined from the MC results, and the temperatures supplied to the simple rate equation model were derived from the average kinetic energy in each subband. The results for the current density and the LH1 subband population are shown in Fig. 3b. Hole-hole scattering was not included in these calculations. The general trend of the results from all four methods is similar at moderate fields. The agreement between the simple particle rate equation approach with $T_{\rm HH} = T_{\rm LH} = T_{\rm latt}$ and the other methods is worst overall, because this method completely neglects carrier heating effects. Given that the hole temperatures lie in the range 100–300K, depending on the field, and that $T_{\rm HH}$ and $T_{\rm LH}$ can differ by up to 100K, this is clearly not a good approximation.

The differences between the MC results and those from the rate equation method with MC-supplied carrier temperatures highlights the influence of the carrier distributions. The MC calculation shows that actual distributions differ considerably from the Fermi-Dirac form. In particular, the HH1 subband has a larger fraction of holes with small $\mathbf{k}_{||}$ than would correspond to a Fermi-Dirac distribution with the same temperature, whilst the opposite applies to the LH1 subband. This is related to the fact that HH-LH mixing

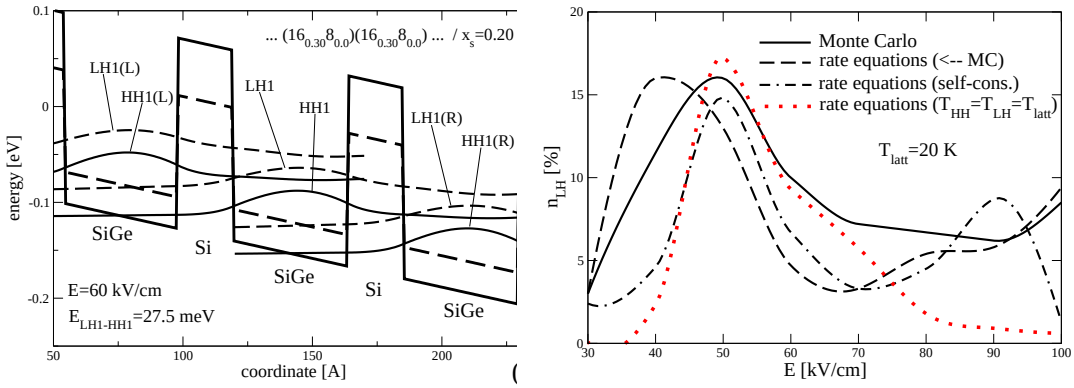

Fig. 3 (a) An example of relevant hole states in a p-SiGe cascade, used in simulations. The wavefunctions of HH and LH states, as well as the valence band edges for heavy and light holes in this strained system, are denoted by solid and dashed lines, respectively. (b) The current density and the LH1 state population vs. electric field dependence in the p-SiGe cascade, calculated using the self-consistent energy balance, Monte Carlo, and particle rate equation methods: the latter with carrier temperatures either set equal to the lattice temperature $T_{latt} = 20$K, or obtained from MC simulations. The sheet hole density is 5×10^{11} cm^{-2} per period.

is small for $\mathbf{k}_{||} \approx 0$, so the wavefunctions of the large-quantization mass heavy holes are then best confined inside wells (and hence worst coupled to neighbouring wells), while the light hole states are most leaky for $\mathbf{k}_{||} \approx 0$. In practice, of course, this latter approach is not very useful, since it requires a prior run of the full Monte Carlo simulation, and yet provides no additional information. Closer correlation between the MC and self-consistent rate equations methods may be anticipated if intrasubband hole-hole scattering were included in the MC algorithm [35], which would result in simulated carrier distributions closer to the Fermi-Dirac form.

4 Conclusion In summary we reviewed the method for physical modelling and describe its application to design and optimisation of mid-infrared and terahertz, GaAs, GaN, SiGe cascade structures. A self-consistent energy balance method for the simulation of electron transport in GaAs/AlGaAs and GaN/AlGaN and hole transport in p-Si/SiGe quantum cascade structures has been developed and used to study carrier dynamics in the structures. The scattering mechanisms included in the model are electron-LO phonon, electron-electron in n-type structures. Particularly, for GaAs THz QCL interface roughness and impurity scattering mechanisms are included as well. The alloy disorder, acoustic and optical phonon scattering, and hole-hole scattering are included in p-type structures, accounting for the in-plane anisotropy of both the hole subband structure and the scattering rates.

The calculation for the GaAs-based QCLs is in very good agreement with the experimental data. In a prototype of GaN and SiGe-based THz cascade structures calculation shows that the lasing action of such structures is feasible, however their realisation is still technologically challenging process.

Acknowledgements This work is supported by EPSRC (UK), Royal Society(UK) ORS(UK) and DARPA (USA).

References

[1] R. Köhler, A. Tredicucci, F. Beltram, H. E. Beer, E. H. Linfield, A. G. Davies, D. A. Ritchie, R. C. Iotti, F. Rossi, Nature **417**, 156 (2002).
[2] B.S. Williams, S. Kumar, Q. Hu, and J. L. Reno, Electr. Lett. **40**, (2004).
[3] G. Scalari, S. Blaser, L. Ajli, J. Faist, H. E. Beer, E. H. Linfield, and A. G. Davies, Phys. Rev. Lett., **93**, 237403 (2004).
[4] B.S. Williams, S. Kumar, H. Callebaut, Q. Hu, and J. L. Reno, Appl. Phys. Lett. **83**, 5142 (2003).
[5] S. Kumar, B.S. Williams, S. Kohen, Q. Hu, and J. L. Reno, Appl. Phys. Lett. **84**, 2494 (2004).

[6] S. Barbieri, J. Alton, H. E. Beer, J. Fowler, E. H. Linfield, and D. A. Ritchie, Appl. Phys. Lett. **85**, 1674 (2004).
[7] H. Page, C. Backer, A. Robertson, G. Glastre, V. Ortiz, and C. Sirtori, Appl. Phys. Lett. **78**, 3529 (2001).
[8] C. Pflügl, W. Schrenk, S. Andres, G. Strasser, C. Becker, C. Sirtori, Y. Bonetti, and A. Muller, Appl. Phys. Lett. **83**, 4698 (2003).
[9] S. Andres, W. Schrenk, E. Gornik, and G. Strasser, Appl. Phys. Lett. **80**, 1864, (2002).
[10] H. Page, S. Dhillon, M. Calligaro, C. Becker, V. Ortiz, and C. Sirtori, IEEE J. Quantum. Elect. **40**, 665 (2004).
[11] M. Beck, D. Hofstetter, T. Aellen, J. Faist, U. Oestrele, M. Illegams, E. Gini and H. Melchoir, Science **295**, 301 (2001).
[12] V. Spagnolo, G. Scamarcio, H. Page, and C. Sirtori, Appl. Phys. Lett. **84**, 3690 (2004).
[13] M. S. Vitiello, G. Scamarcio, V. Sapgnolo, B. S. Williams, S. Kumar, Q. Hu, and J. L. Reno., submitted to Appl. Phys. Lett.
[14] R. C. Iotti, and F. Rossi, Phys. Rev. Lett. **87**, Art. No. 146603 (2001).
[15] R. Köhler, R. C. Iotti, A. Tredicucci, F. Rossi, Appl. Phys. Lett., **79**, 3920 (2001).
[16] H. Callebaut, S. Kumar, B. S. Williams, and Q. Hu, Appl. Phys. Lett. **84**, 645 (2004).
[17] O. Bonno, J.-L Thobel, and F. Dessenne, J. Appl. Phys. **97**, 043702 (2005).
[18] S.-C. Lee and A. Wacker, Phys. Rev. B, **66**, 245314 (2002).
[19] S.-C. Lee and A. Wacker, Appl.Phys. Lett. **83**, 2506 (2003).
[20] D. Indjin, P. Harrison, R. W. Kelsall, Z. Ikonić, Appl. Phys. Lett., **81**, 400 (2002).
[21] P. Harrison, D. Indjin, R. W. Kelsall, J. Appl. Phys. **92**, 6921 (2002).
[22] D. Indjin, P. Harrison, R. W. Kelsall, Z. Ikonić, Appl. Phys. Lett., **82**, 1347 (2003).
[23] V. D. Jovanović, D. Indjin, Z. Ikonić, P. Harrison, Appl. Phys. Lett., **84**, 2995 (2004).
[24] Z. Ikonić, R. W. Kelsall, and P. Harrison, Phys. Rev. B **69**, Art. No. 235308 (1–9) (2004).
[25] Z. Ikonić, P. Harrison, and R. W. Kelsall, J. Appl. Phys., **96**, 6803 (2004).
[26] L. Friedman, R. A. Soref, G. Sun, and Y. Lu, IEEE J. Select. Topics Quantum Electron. **4**, 1029 (1998).
[27] G. Dehlinger, L. Diehl, U. Gennser, H. Sigg, J. Faist, K. Ensslin, D. Grutzmacher, and E. Muller, Science **290**, 2277 (2000).
[28] S. A. Lynch, R. Bates, D. J. Paul, D. J. Norris, A. G. Cullis, Z. Ikonić, R. W. Kelsall, P. Harrison, D. D. Arnone, and C. R. Pidgeon, Appl. Phys. Lett. **81**, 1543 (2002).
[29] R. Bates, S. A. Lynch, D. J. Paul, Z. Ikonić, R. W. Kelsall, P. Harrison, S. L. Liew, D. J. Norris, A. G. Cullis, W. R. Tribe, and D. D. Arnone, Appl. Phys. Lett. **83**, 4092 (2003).
[30] M. S. Vitiello, V. Sapgnolo, G. Scamarcio, B.S. Williams, S. Kumar, Q. Hu, J. L. Reno., 6th Int. conference om Midinfered optoelectronics and Materials and Devices, St Petesburg, Russia, 28 June, 2004.
[31] D. Indjin, Z. Ikonić, V. D. Jovanović, N. Vukmirović, P. Harrison, and R. W. Kelsall, submitted to Semicond. Science Technol.
[32] J. Faist, D. Hofstetter, M. Beck, T. Aellen, M. Rochat, S. Blaser, IEEE J. Quantum Electr. **38** 533, (2002).
[33] D. Indjin, A. Mirčetić, P. Harrison, R. W. Kelsall, Z. Ikonić, V. D. Jovanović, V. Milanović, M. Giehler, R. Hey, H. T. Grahn, 27^{th} Int. Conf. Phys. Second. (ICPS-27), 26–30 July 2004, Flagstaff, Arizona, USA.
[34] V. D. Jovanović, Z. Ikonić, D. Indjin, P. Harrison, V. Milanović, R. A. Soref, J. Appl. Phys. **93**, 3194 (2003).
[35] Z. Ikonić, R. W. Kelsall, P. Harrison, Phys. Rev. B, **69**, Article No, 235308 (2004)